Sensitive Noninvasive Acoustic Detection and Multilateration of Rib Fractures from Simulated Behind Armor Blunt Trauma

Diana D. Tarakhovsky[1], Hesham Aldhaibani[1], Robert MacDonald[1], Katerena R. Sirhan[1], Katarzyna Ochocki[1], Aisha Mazloum[1], Abdul Dannaoui[1], Souren Moradi[1], Karin A. Rafaels[2], Cameron R. 'Dale' Bass[1]

[1]Biomedical Engineering, Wayne State University, USA
[2]US DEVCOM Army Research Laboratory, USA

ABSTRACT

This study uses noninvasive acoustic sensors placed in contact with skin, without being mounted to bone, to investigate rib fractures from simulated behind-armor blunt trauma (BABT) impacts. The objectives were to determine fracture using acoustic sensor signals and to locate where and when the initial fracture occurred using a multilateration algorithm. Using a gas gun, an indenter was accelerated towards the impact site at velocities intended to cause single rib fractures. Testing included five cadaveric, eviscerated porcine torsos in forty-seven repeated impacts to the left and right lateral mid-thorax. Porcine torsos were selected due to their high anatomical congruence with the human thoracic structure, providing a relevant surrogate model for human rib fracture behavior. The multilateration algorithm used known sensor location coordinates, first acoustic emission times, initial peak voltage of sensor emissions, and the speed of sound through soft tissue to locate the initial fracture. Sensor data were collected at high sampling rates to ensure accurate capture of acoustic emissions. Localization results were validated against post-impact X-rays, anatomical inspection, and rib projections. This study proves the practicality of noninvasive acoustic sensors for real time fracture detection. The multilateration algorithm shows promise to improve and validate models of skeletal fracture and increase our understanding of injury mechanisms.

This paper is a student paper from the 20th Injury Biomechanics Symposium. It is preliminary work, has not been peer reviewed, and should not be cited because it is a work in progress.

INTRODUCTION

A detailed understanding of injury mechanisms, particularly the initiation and propagation of fractures following blunt trauma, is essential for advancing injury risk assessments and improving the design of protective equipment such as armor plates. This study focuses on predicting how, when, and where initial rib fractures occur after impact. Previous studies have mounted acoustic sensors directly to bone to determine initiation and location of microcrack fractures (O'Toole et al., 2013). The effect of the tissue disruption and the treatment of the bone/ sensor interface is unknown. This study uses noninvasive acoustic sensors placed in contact with skin, without being mounted to bone, to investigate rib fractures from simulated BABT impacts. This research investigates a technique to noninvasively determine the initiation and location of a crack following impact.

METHODS

Eight acoustic hydrophone sensors (Teledyne Reson, Underwater Acoustics, Daytona Beach, FL, USA) were mounted with sutures onto the porcine skin, over the ribs, in a known position relative to the ribs (Figure 1). Hydrophone sensors were selected because of their larger frequency band and durability in a biological environment compared to traditional acoustic emission sensors. To improve acoustic transmission between the sensors and the skin, ultrasound gel was applied. Using a gas gun, a 200-gram polycarbonate projectile (Op ‘t Eynde et al., 2020) with a rounded, domed impact surface was accelerated towards the impact site, located between ribs seven and nine, at velocities intended to cause single rib fractures. Hydrophone sensors were placed in a circular pattern roughly 70 to 100 mm from the center of the impact site. Five porcine cadaveric surrogates were cut along the transverse plane at the level of the floating ribs, exposing the internal thoracic cavity. Forty-seven impact tests were conducted to the left and right lateral mid-thorax. Indenter velocity was increased each impact until fracture occurred. Palpation of the ribs, along with analysis of the acoustic sensor and video data, was used to determine whether fractures occured. Data from the acoustic sensors were collected at a frequency of 600 KHz using PicoScope (Pico Technology, PicoScope 5444D, Tyler, Texas, USA). Video data from two high-speed cameras (Phantom V1212, Vision Research, Wayne, NJ, USA) were collected at a framerate of 10,000 fps. Camera one was placed in direct line of the gas gun, with the viewpoint of figure one, and camera two was placed with a clear view into the thoracic cavity.

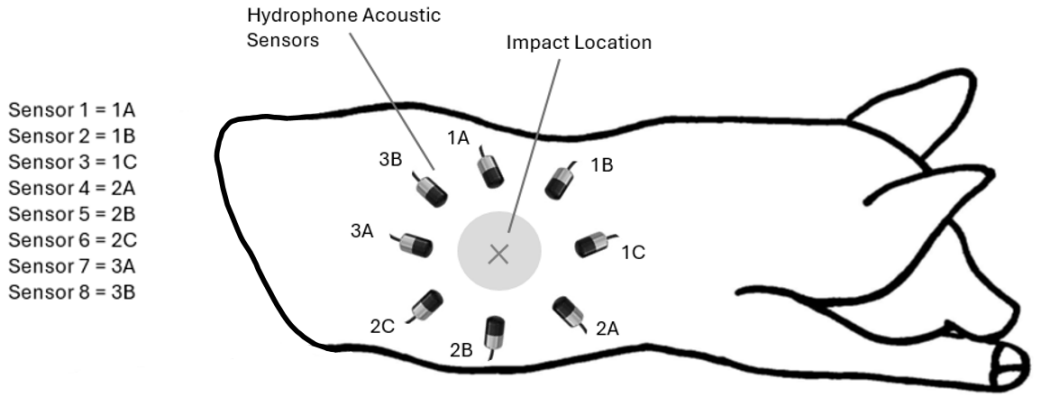

This paper is a student paper from the 20th Injury Biomechanics Symposium. It is preliminary work, has not been peer reviewed, and should not be cited because it is a work in progress.

Figure 1: Test setup and sensor schematic. The positioning of the swine was on the edge of the table with its right side facing the impactor.

First Acoustic Emission Times

Fractures generate bursts of activity from elastic waves that the acoustic sensors detect as peaks in the signal. It was assumed that sensors closer to the fracture origin had quicker emission times and higher voltage spikes. DADiSP (a numerical computing environment, DSP Development Corporation) was used to analyze and filter data. Filtering techniques included a Butterworth filter and time-reversed IIR filters to remove noise and enhance signal clarity. Signals were preprocessed with function setnavalue, and the levelcross function was applied to identify threshold crossings associated with fracture onset. The first fracture acoustic emission was identified as the point when the voltage exceeded eight times the sensor noise pre-test threshold. Any signal emitted before the fracture's initiation was filtered out, and the first highest voltage peak was used to pinpoint the exact time at which the fracture began.

If the voltage recorded by a sensor did not exceed eight times the standard deviation of the pre-test noise, it was concluded that the sensor did not detect a fracture. If none of the sensors registered a signal meeting this threshold during a test, it was determined that no fracture had taken place. Because the objective was to continue applying impacts with increasing velocities until a fracture occurred, some porcine cadavers were subjected to as many as eight impacts.

Sensor Positions

The distance between each sensor and the estimated center of impact was measured manually, following the surface curvature of the swine. Using ImageJ (Schneider et al., 2012), sensor angles were calculated with the estimated point of impact being the axis of measurement. With known distances and angles for every sensor, trigonometric calculations (MATLAB R2023a) were used to obtain positional 2-D coordinates of every sensor relative to the impact location.

Multilateration Algorithm

The multilateration algorithm used known sensor location coordinates, first acoustic emission times, initial peak voltage of sensor emissions, and the speed of sound (1540 m/s) through soft tissue (Feldman et al., 2009) to locate the initial fracture (Equation. 2). The algorithm is based on Euclidean geometry, time of arrival distances, and the fundamental physics formula of speed × time equals the distance (Equation. 1). For each sensor *i*, the squared distance between the fracture location ($X_{Fracture}$, $Y_{Fracture}$) and the sensor position (X_i , Y_i) was calculated. The spatial distance was compared to the time-based distance, determined by the difference between the known fracture time and the first emission time (delta T), multiplied by the speed of sound *C*. The sum for each sensor *i* was multiplied by the initial peak voltage (V). The total summation (Equation. 4) was minimized through optimization (GRG nonlinear engine) with conditions that the real-time fracture had occurred before the first acoustic emission time (Equation. 3). Since sound waves

This paper is a student paper from the 20th Injury Biomechanics Symposium. It is preliminary work, has not been peer reviewed, and should not be cited because it is a work in progress.

travel with a delay through soft tissue, the actual fracture occurred before the sensors detected the signal, which was accounted for with this constraint.

$$\sqrt{(\Delta X)^2 + (\Delta Y)^2} = C \times (\Delta T) \quad (1)$$

$$(X_{Fracture} - X_i)^2 + (Y_{Fracture} - Y_i)^2 - \left(C \times (T_{known} - T_{unknown})\right)^2 \quad (2)$$

$$T_{unknown} \leq T_{known} \quad (3)$$

$$\sum_{i=1}^{8} V_i \times \left[(X_{Fracture} - X_i)^2 + (Y_{Fracture} - Y_i)^2 - \left(C \times (T_{known} - T_{unknown})\right)^2\right]^2 = Total\ Sum \quad (4)$$

RESULTS

The multilateration results provided an estimate of the first fracture locations. Effects from rib thickness, length, curvature, and the thickness of sensors were considered. These factors can affect the propagation speed and path of acoustic waves, potentially introducing small deviations in the calculated locations. Since precise locations of the sensors relative to the ribs in the X-ray images could not be easily determined, it was not possible to directly assess the absolute accuracy of the fracture localization. With only 2-D rib projections available, estimated fracture locations were interpreted relative to even-numbered ribs on a coordinate grid.

Table 1: Multilateration Data

Sensor	Sensor positions (m)		Fracture location		ΔT (s)		Sum × Initial peak	Total Summation
	X_i	Y_i	X	Y	T_{known}	$T_{unknown}$		
1	-0.0378	0.05041	-0.0373	-0.0042	0.002737	0.002709	0.00014402	0.00483563
2	0.05601	0.04682			0.002763		0.00102324	
3	0.11663	-0.0093			0.002842		0.00185598	
4	0.06935	-0.0509			0.002809		0.00129369	
5	0.02622	-0.0681			0.002741		0.00039161	
6	-0.0323	-0.0506			0.002736		2.2756E-05	
7	-0.072	-0.0414			0.002746		9.6207E-05	
8	-0.0633	-0.0092			0.002724		8.134E-06	

Table 1: Multilateration data results of Subject one, left side. The sensor positions and *Tknown* columns represent the known data. The fracture location and *Tunknown* represent the unknown data. The total summation value represents what was minimized in the optimization process.

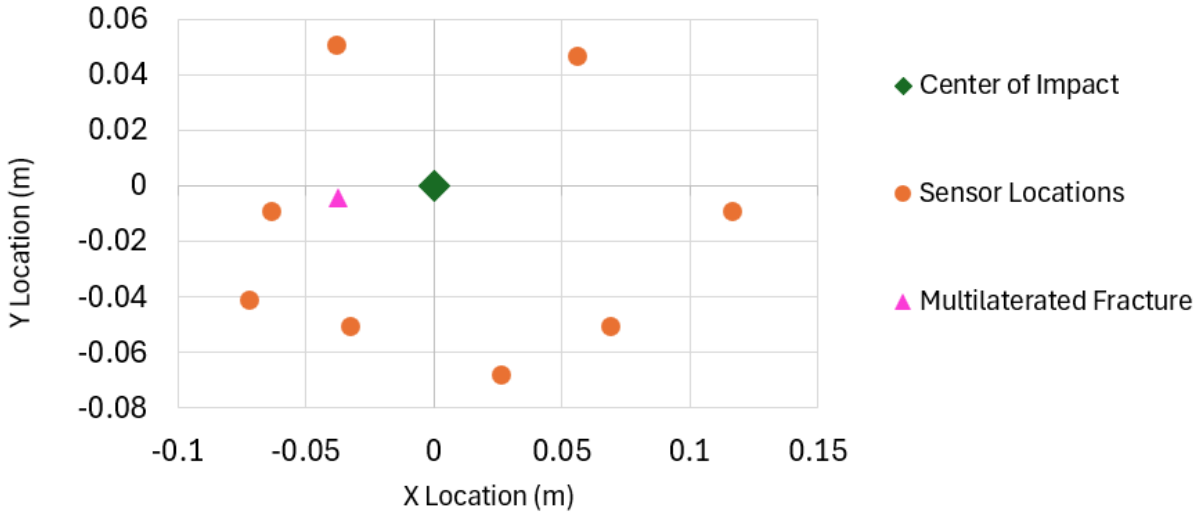

Figure 2: Multilateration results of the initial fracture location for the first swine's left ribs. The pink triangle represents the initial fracture located at (-0.0373, -0.0042) from the center of impact (0,0), represented by the green diamond. Orange circles represent sensor locations.

Table 2: Multilateration Data

Sensor	Sensor positions (m)		Fracture location		ΔT (s)		Sum × Initial peak	Total Summation
	X_i	Y_i	X	Y	T_{known}	$T_{unknown}$		
1	0.02396	0.0679	-1.40E-02	-5.66E-02	0.001563	0.00143352	2.58E-03	1.54E-02
2	0.06532	0.02783			0.001507		8.63135E-06	
3	0.07618	-0.06			0.001584		0.01009878	
4	0.02788	-0.0707			0.001445		0.00208037	
6	-0.0663	-0.0329			0.00146		0.00052486	
7	-0.0989	0.02502			0.001515		6.152E-05	
8	-0.0378	0.05161			0.001502		1.74296E-05	

Table 2: Multilateration data results of Subject one, right side.

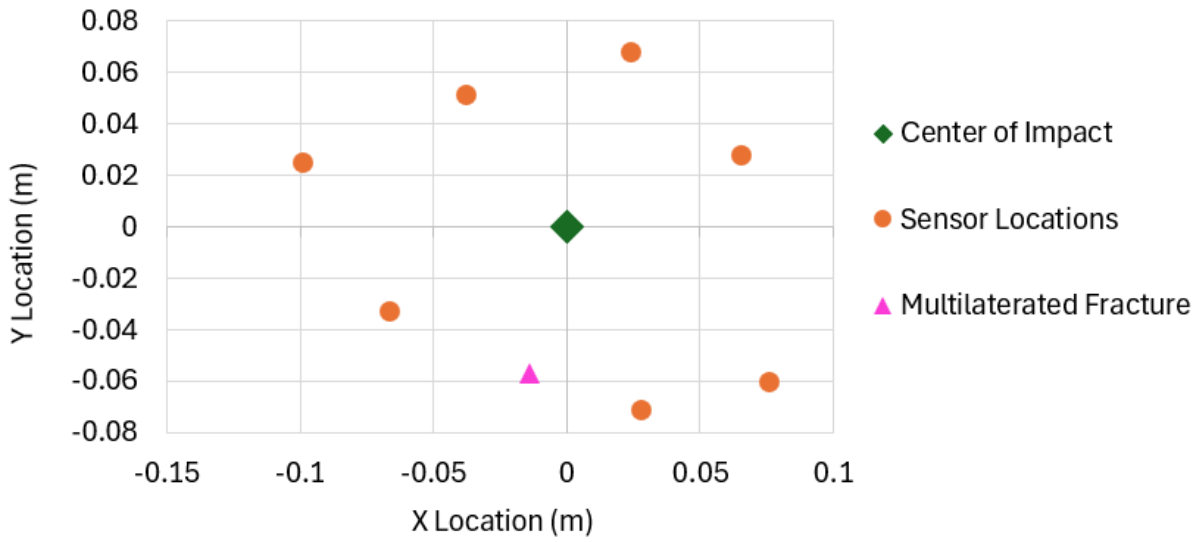

Figure 3: Multilateration results of the initial fracture location for the first swine's right ribs. The fracture is located at (-1.40E-02, -5.66E-02) from the center of impact.

Table 3: Multilateration Data

Sensor	Sensor positions (m)		Fracture location		ΔT (s)		Sum × Initial peak	Total Summation
	X_i	Y_i	X	Y	T_{known}	$T_{unknown}$		
1	0.03686	0.06185	0.0637288	-0.10902988	0.002851	0.002732862	4.33112E-05	9.75E-03
2	0.07509	0.02455			0.002808		0.000303425	
3	0.09178	-0.0314			0.002789		1.85924E-05	
4	0.01398	-0.0696			0.002733		0.004118067	
5	-0.0408	-0.0581			0.002834		0.000802313	
6	-0.082	-0.0021			0.002864		0.0001885	
7	-0.0689	0.07113			0.002943		0.004280604	

Table 3: Multilateration data results of Subject two, right side.

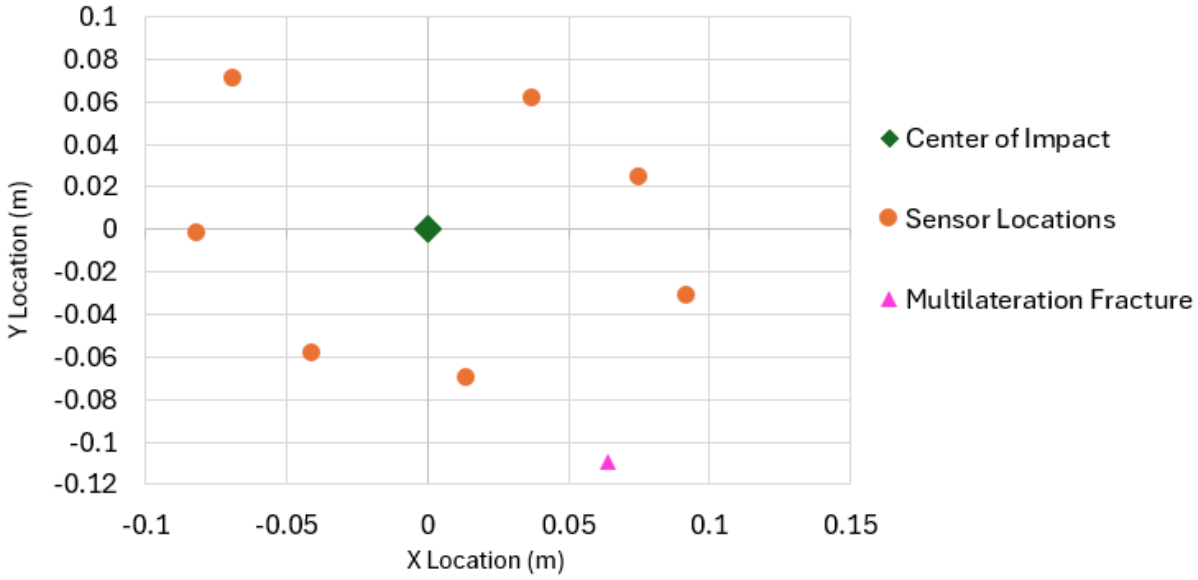

Figure 4: Multilateration results of the initial fracture location for the second swine's right ribs. The fracture is located at (0.0637288, -0.10902988) from the center of impact.

The rib locations were found on a 2-D projection based on sensor locations. Sensors were in the positioned on specific ribs for each test, arranged on every other rib between ribs four to twelve. Two sensors were positioned on the anterior and posterior ends of ribs six, eight, and ten. The sensors attached to rib four and twelve were positioned medial of the rib. MATLAB was used to create 2-D projections of sensor locations with an overlay of fracture location in relation to the target rib (rib eight).

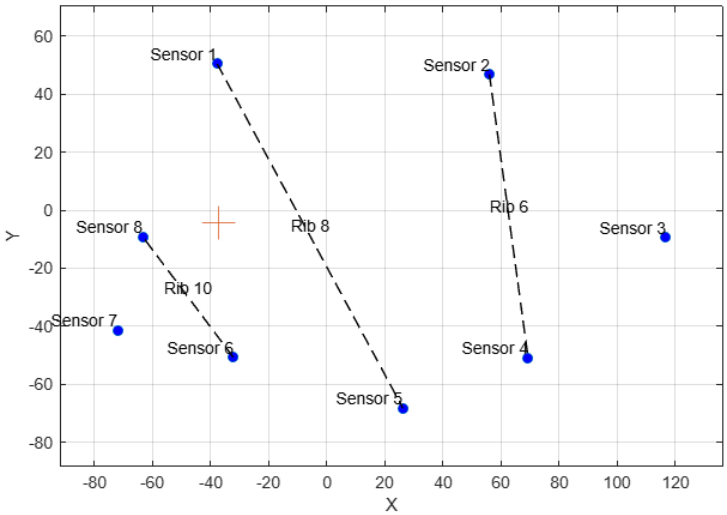

Figure 5: 2-D rib projections for the first swine's left ribs. The sensors on rib six had a distance of 98.59 mm, rib eight had 134.71 mm, and rib ten had 51.70 mm. The projected multilateration fracture appears to be on rib nine.

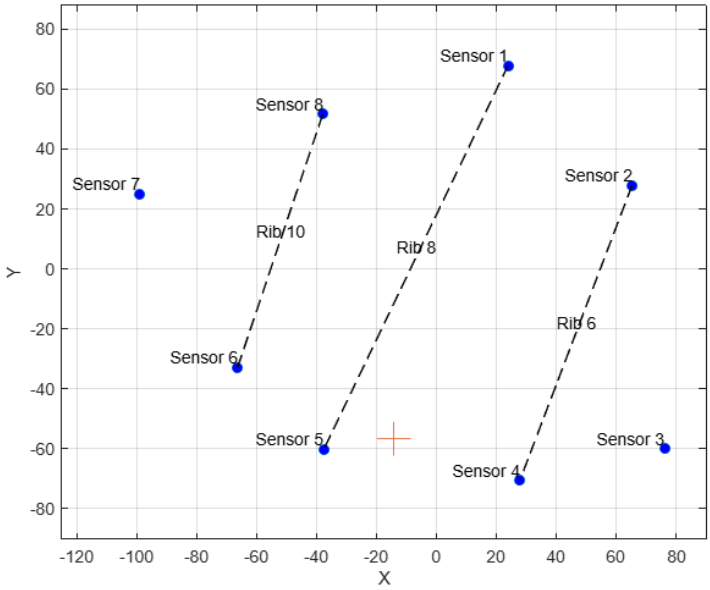

Figure 6: Two-dimensional rib projections for the first swine's right ribs. The sensors on rib six had a distance of 105.40 mm, rib eight had 142.15 mm, and rib ten had 89.15 mm. The projected multilateration fracture appears to be on rib seven.

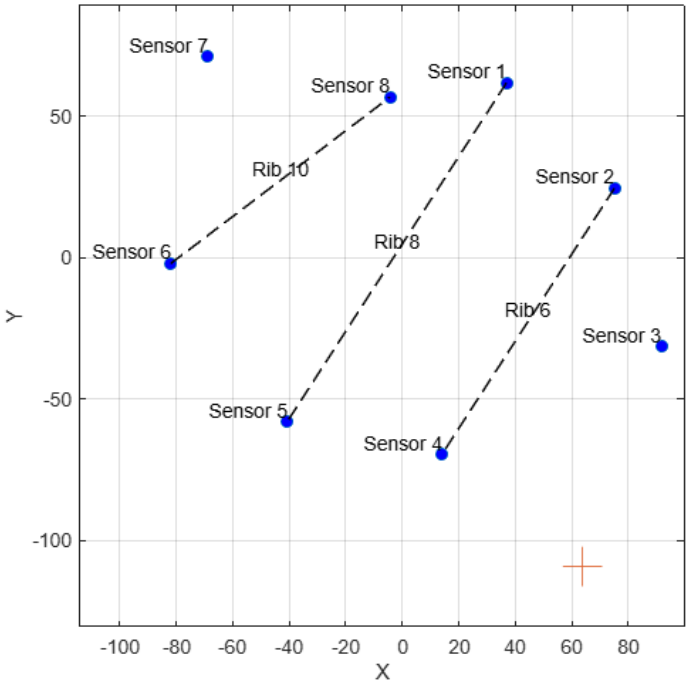

Figure 7: Two-dimensional rib projections for the first swine's right ribs. The sensors on rib six had a distance of 112.25 mm, rib eight had 142.9 mm, and rib ten had 97.50 mm. The projected multilateration fracture appears to be out of range from the sensors.

X-rays were taken of each rib cage bisection. Ribs were numbered consecutively from superior (one) to inferior. Using this nomenclature, most fracture localizations ranged from ribs seven to nine, aligning with the intended shot location centered around the eighth rib.

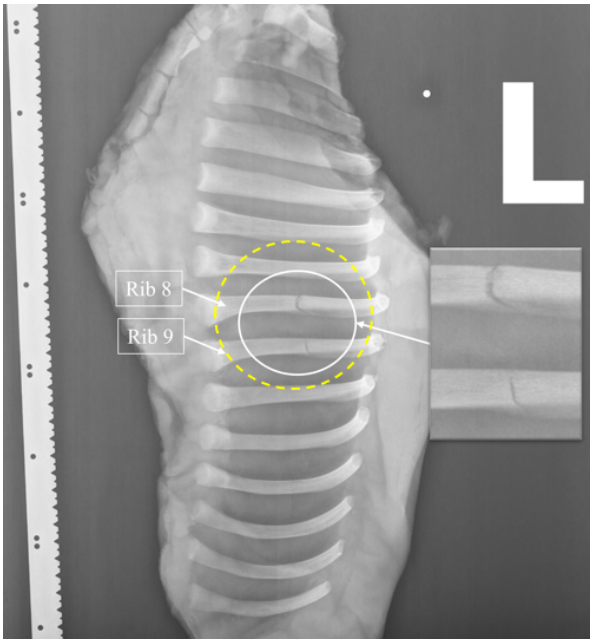

Figure 8: X-ray of the first swine's left side. There is a transverse fracture on rib eight and a hairline fracture on rib nine. The checkered yellow circle represents the location of the impact.

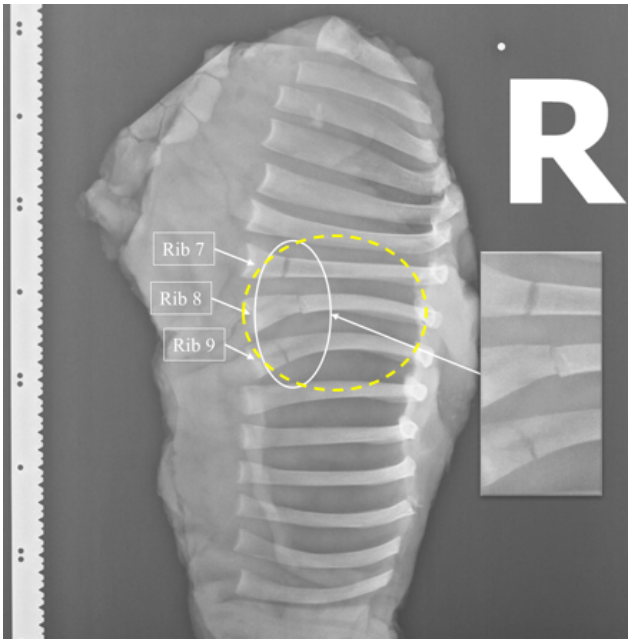

Figure 9: X-ray of the first swine's right side. There are transverse fractures on ribs seven and nine and a displaced oblique fracture on rib eight.

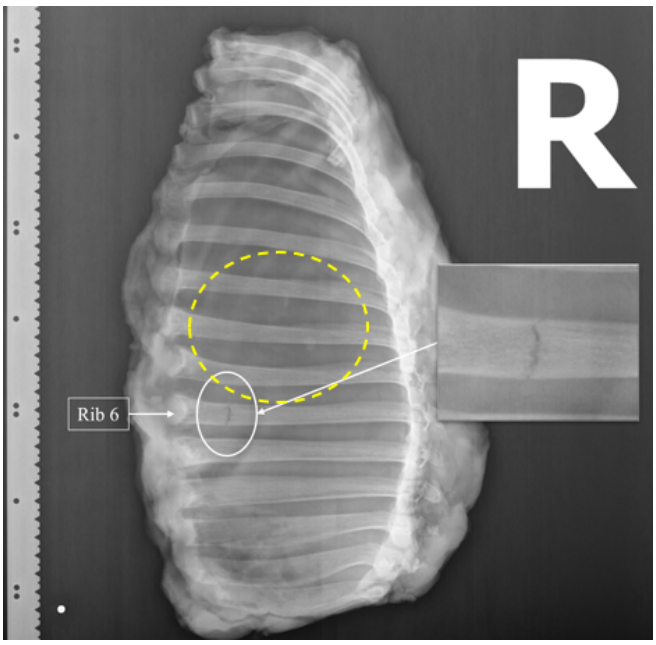

Figure 10: X-ray of the second swine's right side. There is a transverse fracture on rib six.

For subject one left side, the algorithm projected the fracture on rib nine, closely matching the confirmed hairline fracture on rib nine. Although another fracture was on rib eight, the sequence of fracture events remains uncertain. However, the result suggests the model identified the correct region of initial fracture since the sensors with the earliest emission times were closer to rib nine than eight. For subject one right side, the projection appeared on rib seven, which correlated with a transverse fracture on that rib. However, with additional fractures on ribs eight and nine, the order in which they occurred is not certain. Sensor four, which was closest to rib seven, had the earliest emission time and the highest initial peak voltage. For subject two right side, the algorithm's fracture prediction was out of range of the sensor site, closest to sensor 4 at 63.47 mm away. This mislocalization may stem from overlapping acoustic signals or ambiguous peak voltage patterns.

DISCUSSION

This study demonstrates an approach for fracture detection using noninvasive acoustic sensors. The oscillations in the fracture, formed at the highest point of stress, produce a sound that was detected by the sensors. As the fracture progressed, the acoustic emissions increased, which provided a detailed signature of fracture progression. The sensors closer to the fracture origin detected the signal sooner than those farther away. The delay between the real-time fracture occurrence and time the sensors picked up data was due to the fracture's oscillations travelling through soft tissue at an estimated velocity of 1540 m/s. For most impacts, the first fracture occurred under the shot location. After dissection, it was observed that a few subjects had a hairline fracture on the rib directly under the impact location, but the algorithm identified the first fracture,

an oblique nondisplaced fracture, on a different rib. It is possible that the signal of the hairline fracture under the impact location did not exceed the threshold or could have been pre-existing since the swine witnessed multiple impacts.

The multilateration algorithm provided localization of fractures, showing potential in injury biomechanics. However, the algorithm is limited to identifying only the first fracture, as it cannot isolate microfractures due to overlapping signals. Incorporating initial peak voltage into the summation improved optimization accuracy by giving more weight to stronger signals, as they are closer to the fracture location. The speed of sound has a great influence on the optimization, as it scales the time component and is several orders of magnitude larger than the temporal and spatial variables. Acoustic wave propagation following fracture include a combination of compressional, shear, surface, and plate waves. The contribution of each wave mode depends on the sensor's position and orientation with respect to the fracture site. In trials where the speed of sound was allowed to vary, the solver often converged on unrealistically low values for c, resulting in incorrect fracture localization, often near the center of the sensor array. Fixing c at a physiological value (e.g., 1540 m/s) improved accuracy in some instances but reduced flexibility in others. The assumption that all sensors detect the same fracture event may not hold in complex or noisy trials, especially when multiple wave modes overlap. In such cases, the model may misinterpret overlapping emissions from separate fracture points or reflect secondary waves, leading to false identification of fracture location.

Fundamentally, these limitations arise from uncertainties in the initial waveform time location for two reasons. First, for practical purposes, the arrival time of acoustic radiation can only be identified when the signal rises above the fundamental noise in the sensor and recording system. Second, in the current experimental arrangement there are geometric and material uncertainties, including a variable compressive speed of sound between crack initiation and the sensor location and the intrinsically three-dimensional geometry of the chest. These limitations will be assessed and addressed in future studies.

Due to the limitations of X-rays, not all microscopic fractures can be detected, which is why palpating for displacement on the rib surfaces was necessary for accurate results (Pinto et al., 2018). The size of tissue thickness affects fractures and velocity speed. However, skin thickness measurements were not obtained, so they could not be factored into the multilateration process. Despite these limitations, this method of multilateration shows promise for improving noninvasive injury diagnostics in any injury context. This algorithm could be used as a tool to address where the most common places of fracture take place, helpful in sports injuries and injury biomechanics research to understand injury mechanisms.

CONCLUSIONS

This research demonstrated that noninvasive acoustic sensors can effectively detect and localize rib fractures caused by simulated behind-armor blunt trauma impacts. By applying a multilateration algorithm based on time differences and acoustic signal, the study localized fractures noninvasively. The approach identified initial fracture locations across multiple test conditions using cadaveric swine torsos as anatomical surrogates. These results show that a

noninvasive approach offers an alternative to sensors being directly mounted on bone. The findings focus the potential for real-time monitoring of skeletal injuries in research and operational settings. The method developed provides a foundation for further improving injury models and enhancing protective equipment designs. Future studies will focus on refining the multilateration algorithm with a 3D mapping of sensors and expanding testing to human cadaveric models. Additional efforts will aim to account for complex acoustic wave interactions within biological tissues and improve filtering of overlapping signals.

ACKNOWLEDGEMENTS

A special thank you goes to my mentors, Dr. Cameron 'Dale' Bass and Dr. Karin Rafaels, for giving me the opportunity to work on this project and giving me great guidance. An additional thank you goes to the Biomechanics Injury Research team and Wayne State University for providing me with laboratory usage and additional guidance and support.

REFERENCES

FELDMAN, M.K., KATYAL, S., BLACKWOOD, M.S. (2009). US Artifacts. *RadioGraphics*, 29(4), 1179–1189.

PINTO, A., BERRITTO, D., RUSSO, A. (2018). Traumatic Fractures in Adults: Missed Diagnosis on Plain Radiographs in the Emergency Department. *Acta Biomedica*, Vol. 89, Supplement: 111–123.

O'TOOLE, J., CREEDON, L., HESSION, J., MUIR, G. (2013). Hyperbolic Source Location of Crack Related Acoustic Emission in Bone. *Journal of Biomechanical Engineering*, 135(1), 011006.

SCHNEIDER, C.A., RASBAND, W.S., ELICEIRI, K.W. (2012). NIH Image to ImageJ: 25 years of image analysis. *Nature Methods*

MATHWORKS INC. (2023). MATLAB release notes for R2023a [Software]. Retrieved from https://www.mathworks.com/help/release-notes/r2023a.html"

OP 'T EYNDE, J., ECKERSLEY, C.P., SALZAR, R.S., STEMPER, B.D., SHENDER, B.S., BENTLEY, T.B., BASS, C.R. (2020). Behind Armour Blunt Trauma (BABT) Indenter Simulating High-Velocity Impacts from Rifle Rounds on Hard Body Armour. Proceedings of the Personal Armour Systems Symposium, 2020.